LA-UR -85-3276

CONF-850763 -1

RECEIVED BY OSTI OCT 09 1985

TITLE: THE RELATION BETWEEN FINITE ELEMENT METHODS AND NODAL METHODS IN TRANSPORT THEORY

LA-UR--85-3276

DE86 000761

AUTHOR(S): Wallace F. Walters

SUBMITTED TO: International Seminar on Finite Element and Allied Methods for Reactor Physics and Shielding Calculations
September 18-20, 1985

Los Alamos

Los Alamos National Laboratory
Los Alamos, New Mexico 87545

THE RELATION BETWEEN FINITE ELEMENT METHODS AND NODAL METHODS IN TRANSPORT THEORY

by

Wallace F. Walters
Radiation Transport Group, X-6
P. O. Box 1663, MS B226
Los Alamos National Laboratory
Los Alamos, NM 87545

I. INTRODUCTION

This paper examines the relationship between nodal methods and finite-element methods for solving the discrete-ordinates form of the transport equation in x-y geometry. Specifically, we will examine the relation of three finite-element schemes to the linear-linear[1] (LL) and linear-nodal[2,3] (LN) nodal schemes. The three finite-element schemes are the linear-continuous-diamond-difference[4] (DD) scheme, the linear-discontinuous[5-8] (LD) scheme, and the quadratic-discontinuous (QD) scheme. A brief derivation of the (LL) and (LN) nodal schemes is given in the third section of this paper. The approximations that cause the LL scheme to reduce to the DD, LD, and QD schemes are then indicated. An extremely simple method of deriving the finite-element schemes is then introduced.

Recently, two papers have been published that indicate, in some detail, an interesting form into which the LN equations can be cast.[9,10] It will be shown that the finite-element schemes being considered can be cast into this same "augmented-weighted-diamond" form, and the same algorithm that has been used to solve the LN equations can be used to solve the finite-element equations. For more information on the nodal method in transport theory, an excellent review paper on the subject that is being published should be consulted.[11] In the last section of the paper, a well-logging problem is analyzed using all of the schemes under discussion in this paper. The accuracy of the results are in agreement with the observations made in the paper.

II. PRELIMINARIES

The discrete-ordinates form of the transport equation for direction m and energy group g is

$$\mu_m \frac{\partial \Psi_{m,g}}{\partial x} + \eta_m \frac{\partial \Psi_{m,g}}{\partial y} + \sigma_g \Psi_{m,g} = S_{m,g} \quad , \tag{1}$$

Here $\Psi(x,y,\mu,\eta)$ is the neutron angular flux. σ is the neutron total cross section. S is the driving source for the transport equation and can consist of in-scatter, out-scatter, self-scatter, and fission. μ and η and the x- and y-direction cosines. Hereafter, the subscripts m and g will be suppressed.

The solution to this form of the transport equation will be obtained for all the numerical schemes within the rectangular node or cell bounded by

$$x_L \le x \le x_R \quad ,$$

$$y_B \le y \le y_T \quad ,$$

with

$$\Delta x = x_R - x_L \quad ,$$

$$\Delta y = y_T - y_B \quad ,$$

$$\bar{x} = \frac{x_L + x_R}{2} \quad , \text{ and}$$

$$\bar{y} = \frac{y_T + y_B}{2} \quad .$$

Throughout this paper, L, R, B, T, and A are subscripts such that L = left, R = right, B = bottom, T = top, and A = average. For simplicity in developing the equations for the schemes under consideration, it will be assumed, in all cases, that $\mu,\eta > 0$. That is, the neutron flow is from left to right and bottom to top.

The cell-based Legendre polynomials used by other investigators[1,2] are now introduced

$$P_0(u) = 1 \quad , \tag{2a}$$

$$P_1(u) = \frac{2(u - \bar{u})^2}{\Delta u} \quad , \tag{2b}$$

$$P_2(u) = \frac{6(u - \bar{u})^2}{(\Delta u)^2} - \frac{1}{2} \quad , \tag{2c}$$

where u = x or y. These polynomials exhibit the usual orthogonal properties

$$\int P_\ell(u) P_k(u) du = \delta_{k\ell} \frac{\Delta u}{2k+1} \quad . \tag{3}$$

If the neutron angular flux within the node is given by $\Psi(x,y)$, then

$$\psi_A = \frac{\int_{y_B}^{y_T} dy \int_{x_L}^{x_R} dx P_0(x) P_0(y) \Psi(x,y)}{\Delta x \Delta y} \quad , \tag{4a}$$

$$\psi_x = \frac{3 \int_{y_B}^{y_T} dy \int_{x_L}^{x_R} dx P_1(x) P_0(y) \Psi(x,y)}{\Delta x \Delta y} \quad , \tag{4b}$$

and

$$\psi_y = \frac{3 \int_{y_B}^{y_T} dy \int_{x_L}^{x_R} dx P_0(x) P_1(y) \Psi(x,y)}{\Delta x \Delta y} \quad , \tag{4c}$$

where ψ_A is the average flux in the node, ψ_x is the average x-moment of the flux in the node, and ψ_y is the average y-moment of the flux in the node. In a similar manner, if the source within the node is given by $S(x,y)$, then S_A can be defined as the average source in the node, S_x the average x-moment of the source in the node, and S_y the average y-moment of the source in the node.

If $\Psi(x,y_T)$ is the angular flux on the top edge or face of the node, then

$$\psi_T = \frac{\int_{x_L}^{x_R} P_0(x)\Psi(x,y_T)}{\Delta x} \ , \tag{5a}$$

$$\theta_T = \frac{3\int_{x_L}^{x_R} P_1(x)\Psi(x,y_T)}{\Delta x} \ , \tag{5b}$$

where ψ_T is the average angular flux on the top edge of the node, and θ_T is the average x-moment on the top edge of the node. Similar expressions hold for the moments on the other edges.

At this point, three moment equations of the transport equation are introduced using the quantities defined earlier in this section. If the transport equation is multiplied by $P_0(x) \cdot P_0(y)/\Delta x\Delta y$ and integrated over the node, the balance equation for the average flux ψ_A is obtained

$$\frac{\psi_R - \psi_L}{\epsilon_x} + \frac{\psi_T - \psi_B}{\epsilon_y} + \psi_A = \frac{S_A}{\sigma} \ . \tag{6}$$

If the transport equation is multiplied by $3 \cdot P_1(x) \cdot P_0(y)/\Delta x\Delta y$ and integrated over the node, the balance equation for the average x-moment of flux ψ_x is obtained

$$\frac{3(\psi_R + \psi_L - 2\psi_A)}{\epsilon_x} + \frac{(\theta_T - \theta_B)}{\epsilon_y} + \psi_x = \frac{S_x}{\sigma} \ . \tag{7}$$

If the transport equation is multiplied by $3 \cdot P_0(x) \cdot P_1(y)/\Delta x\Delta y$ and integrated over the node, the balance equation for the average y-moment of the flux ψ_y is obtained

$$\frac{(\theta_R - \theta_L)}{\epsilon_x} + \frac{3(\psi_B + \psi_T - 2\psi_A)}{\epsilon_y} + \psi_y = \frac{S_y}{\sigma} \ . \tag{8}$$

Here, $\epsilon_x = \sigma\Delta x/\mu$ and $\epsilon_y = \sigma\Delta y/\eta$.

These moment equations will be used to simplify terms appearing in the derivation of the nodal equations in the next section. The discontinuous-finite-element equations will be derived directly form these moment equations in the fourth section of this paper.

III. NODAL SCHEMES

The equations for the LL nodal scheme are derived based on linear expansions for the source within the node $S(x,y)$, and fluxes on the edges such as $\Psi(x,y_T)$. These are

$$S(x,y) = S_A P_0(x)P_0(y) + S_x P_1(x)P_0(y) + S_y P_0(x)P_1(y) \quad , \tag{9a}$$

and

$$\Psi(x,y_T) = \psi_T P_0(x) + P_1(x)\theta_T \quad . \tag{9b}$$

If the transport equation is multiplied by $P_0(x)/\Delta x$ and a transverse integration is carried out over x, the resulting one-dimensional equation in y can be solved for the unknown angular flux ψ_T along the top edge

$$\begin{aligned}\psi_T = \psi_B \exp(-\epsilon_y) + P_0(\epsilon_y)\left[S_A\Delta y/n + \frac{\epsilon_y(\psi_L - \psi_R)}{\epsilon_x}\right] \\ + [2P_1(\epsilon_y) - P_0(\epsilon_y)]\left[S_y\Delta y/n + \frac{\epsilon_y(\theta_L - \theta_R)}{\epsilon_x}\right] \quad .\end{aligned} \tag{10}$$

Notice that a linear transverse leakage and source are indicated in this expression.

If the transport equation is multiplied by $3 \cdot P_1(x)/\Delta x$, and a transverse integration is carried out over x, the resulting one-dimensional equation in y can be solved for the unknown x-moment of the angular flux θ_T along the top edge

$$\theta_T = \theta_B \exp(-\epsilon_y) + P_0(\epsilon_y)[S_x\Delta y/n + \frac{3\epsilon_y(2\psi_A - \psi_R - \psi_L)}{\epsilon_x}]$$
$$+ [2P_1(\epsilon_y) - P_0(\epsilon_y)][\frac{3\epsilon_y(2\psi_y - \theta_R - \theta_L)}{\epsilon_x}] \quad . \tag{11}$$

By carrying out the transverse integration over the y variable, similar equations for the unknowns ψ_R and θ_R can be derived. Here

$$P_0(\epsilon) = \frac{(1 - e^{-\epsilon})}{\epsilon} \quad , \tag{12a}$$

and

$$P_1(\epsilon) = \frac{[1 - P_0(\epsilon)]}{\epsilon} \quad . \tag{12b}$$

These four equations, along with the three moment equations for ψ_A, ψ_x, and ψ_y, constitute the LL nodal scheme.

Before reducing the LL equations to the LN equations, it should be noted that the terms in equations for ψ_T and θ_T that appear due to the constant expansion terms can be rewritten using the ψ_A balance equation. In a similar manner, the terms in the equations for ψ_T and θ_T that appear due to the linear expansion terms can be rewritten using the ψ_y balance equation. The rewritten equations are

$$\psi_T = \psi_B \exp(-\epsilon_y) + P_0(\epsilon_y) \times [\epsilon_y\psi_A + \psi_T - \psi_B] + [2P_1(\epsilon_y) - P_0(\epsilon_y)]$$
$$\times [3(\psi_T + \psi_B - 2\psi_A) + \epsilon_y\psi_y] \quad , \tag{13a}$$

and

$$\theta_T = \theta_B \exp(-\epsilon_y) + P_0(\epsilon_y) \times [\epsilon_y \psi_x + (\theta_T - \theta_B)]$$
$$+ [2P_1(\epsilon_y) - P_0(\epsilon_y)] \tag{13b}$$
$$\times \left[3\left(\frac{\epsilon_y}{\epsilon_x}\right) \times (2\psi_y - \theta_R - \theta_L)\right] \quad .$$

The LN equations are obtained by assuming the diamond relation in only the last term in the equation for θ_T. That is,

$$\psi_y = \frac{(\theta_R + \theta_L)}{2} \quad . \tag{14}$$

A similar assumption is made for ψ_x in the θ_R equation. The LN equations are much simpler than the LL equations due to uncoupling of the equations that results from this diamond approximation in the θ equations. Note that this is equivalent to dropping all terms in the θ equations that appear because of linear terms in expansions. The LN equation for θ_T can be solved for ψ_x to obtain

$$\psi_x = \theta_T \cdot \left[\frac{P_1(\epsilon_y)}{P_0(\epsilon_y)}\right] + \theta_B \left[1 - \frac{P_1(\epsilon_y)}{P_0(\epsilon_y)}\right] \quad . \tag{15}$$

A similar expression is obtained for ψ_y from the θ_R equation. In the limit of small Δy, this relation for ψ_x becomes the diamond relation

$$\psi_x = \frac{\theta_T + \theta_B}{2} \quad , \tag{16}$$

and in the limit of large Δy, it becomes the step relation that agrees with the result in the linear-discontinuous (LD) method

$$\psi_x = \theta_T \quad . \tag{17}$$

In Ref. 9, these LN equations were further reduced to an "augmented-weighted-diamond" form. The expressions for ψ_A are of the following form:

$$\psi_A = \left(\frac{1-\alpha_x}{2}\right)\psi_L + \left(\frac{1+\alpha_x}{2}\right)\psi_R - C_{1x}\theta_B + C_{2x}S_x \quad , \tag{18a}$$

and

$$\psi_A = \left(\frac{1-\alpha_y}{2}\right)\psi_B + \left(\frac{1+\alpha_y}{2}\right)\psi_T - C_{1y}\theta_L + C_{2y}S_y \quad . \tag{18b}$$

The constants appearing in these relations depend only on μ, η, Δx, Δy, and σ. Using these expressions in the ψ_A balance equation, ψ_A can be determined, and all outflow quantities can be obtained by simple extrapolations. The computer program using the LN scheme is programmed using this technique to solve the LN equations.

IV. FINITE ELEMENT SCHEMES

It is a simple matter to generate the diamond-difference relations from the nodal equation (13a). First, the Pade' (1,1) expansion is used for the exponent everywhere it appears in this equation. That is

$$\exp(-\varepsilon) = \frac{2-\varepsilon}{2+\varepsilon} \quad . \tag{19}$$

Note that $P_0(\varepsilon)$ and $P_1(\varepsilon)$ become in this approximation

$$P_0(\varepsilon) = \frac{2}{2+\varepsilon} \quad , \tag{20a}$$

and

$$P_1(\varepsilon) = \frac{1}{2+\varepsilon} \quad , \tag{20b}$$

so that

$$2 \cdot P_1(\varepsilon) - P_0(\varepsilon) = 0 \quad .$$

The equation for ψ_T becomes

$$\psi_T = \psi_B \frac{2 - \epsilon_y}{2 + \epsilon_y} + \frac{2}{2 + \epsilon_y} [\epsilon_y \psi_A + \psi_T - \psi_B] \quad . \tag{21}$$

This relation reduces to

$$\psi_A = \frac{\psi_T + \psi_B}{2} \quad , \tag{22}$$

which is the usual diamond-difference relation associated with a linear-continuous finite element in x-y rectangular geometry. This relation along with the balance equation, Eq. (6), constitutes the DD scheme.

The use of the Pade' (1,1) approximation in the LL equations removes the influence of the linear moments of the flux and the source in the determination of the node average flux and the node edge fluxes. It should be clear that the DD scheme is less accurate than all the higher order schemes when linear moments of the flux and source are important and when the Pade' (1,1) approximation is a poor approximation to the exponent. Both of these conditions can occur when the optical thickness of the node (ϵ_x or ϵ_y) becomes large. Notice that the Pade' (1,1) approximation to the exponent is negative for $\epsilon > 0$.

The linear-discontinuous (LD) equations can be obtained from the LL equations (13a) and (13b) with the following assumptions. First, the Pade' (1,2) approximation is used for the exponents appearing in Eq. (13a) for ψ_T. This approximation is

$$\exp(-\epsilon) = \frac{6 - 2\epsilon}{6 + 4\epsilon + \epsilon^2} \quad . \tag{23}$$

Next is assumed that the unknown node-edge linear-flux moments are equal to the node-average linear flux moments. That is

$$\theta_T = \psi_x \quad , \tag{24a}$$

and

$$\theta_R = \psi_y \quad . \tag{24b}$$

These approximations, along with the three balance equations (6), (7), and (8) for ψ_A, ψ_x, and ψ_y, and the approximate equations for ψ_T and ψ_R constitute the LD equations. Notice that the Pade' (1,2) approximation to the exponent is negative for $\varepsilon > 3$.

The scheme referred to as the quadratic-discontinuous (QD) scheme is identical to the LD scheme except for the Pade' approximation used in Eq. (13a). The QD scheme is obtained by assuming the Pade' (2,3) approximation for the exponent in Eq. (13a). This approximation is given by

$$\exp(-\varepsilon) = \frac{60 - 24\varepsilon + 3\varepsilon^2}{60 + 36\varepsilon + 9\varepsilon^2 + \varepsilon^3} \quad . \tag{25}$$

It is important to note that this Pade' approximation to the exponent is always positive for <u>any positive real value of ε</u>. In the next section of this paper, the discontinuous-finite-element schemes will be derived in a more straightforward manner using polynomial expansions and the balance equations.

V. DERIVATION OF DISCONTINUOUS FINITE ELEMENT SCHEMES

First, the equations of the LD scheme will be derived directly from the balance equations, Eqs. 6-8. The LD approximation assumes a linear expansion for the flux $\Psi(x,y)$ within the node

$$\Psi(x,y) = \psi_A P_0(x) P_0(y) + \psi_x P_1(x) P_0(y) + \psi_y P_0(x) P_1(y) \quad . \tag{26}$$

Recall that, in discontinuous methods, the flow is discontinuous on the inflow edges, but continuous at the outflow edges. This implies that

$$\theta_R = \psi_y \quad , \tag{27a}$$

and

$$\psi_y = \psi_T - \psi_A \quad . \tag{27b}$$

If the expression for θ_R is substituted into the balance equation for ψ_y, Eq. (8), then

$$\frac{3(\psi_T + \psi_B - 2\psi_A)}{\epsilon_y} + \psi_y(1 + \frac{1}{\epsilon_x}) - \frac{\theta_L}{\epsilon_y} = \frac{S_y}{\sigma} \quad . \tag{28}$$

Now, substitute the expression (27b) into Eq. (28) to obtain

$$3(\psi_T + \psi_B - 2\psi_A) + \epsilon_y(\psi_T - \psi_A)(\frac{1 + \epsilon_x}{\epsilon_x}) - \frac{\theta_L \epsilon_y}{\epsilon_x} = \frac{S_y \Delta y}{\eta} \quad . \tag{29}$$

Rearranging this equation yields the "augmented-weighted-diamond" form associated with the LD approximation

$$\psi_T = (2 - f_y)\psi_A - (1 - f_y)\psi_B + \frac{f_y}{1 + \epsilon_x} \cdot [\theta_L + \frac{S_y \Delta x}{\mu}] \quad . \tag{30}$$

$$f_y = \frac{\epsilon_y(1 + \epsilon_x)}{3\epsilon_x + \epsilon_y(1 + \epsilon_x)} \quad . \tag{31}$$

A similar expression can be obtained for the x coordinate carrying out similar operations on the ψ_x equation, Eq. (7). These expressions, along with the balance equation of ψ_A, constitute the equations of the linear-discontinuous (LD) scheme.

The quadratic discontinuous approximation makes the assumption of a quadratic expansion within the node

$$\begin{aligned}\Psi(x,y) = \psi_A P_0(x)P_0(y) + \psi_x P_1(x)P_0(y) + \psi_y P_0(x)P_1(y) \\ + \psi_{xx} P_2(x)P_0(y) + \psi_{yy} P_0(x)P_2(y) \quad .\end{aligned} \tag{32}$$

Here ψ_{uu} is the second moment of the flux within the cell with u = x or y. In this approximation, the assumption of a linear source within the node and a linear flux on the edges of the node are retained. With these assumptions, the second moment balance equations are

$$\frac{5(\psi_R - \psi_L - 2\psi_x)}{\varepsilon_x} + \psi_{xx} = 0 \quad , \tag{33a}$$

and

$$\frac{5(\psi_T - \psi_B - 2\psi_y)}{\varepsilon_y} + \psi_{yy} = 0 \quad . \tag{33b}$$

From the quadratic flux expansion

$$\psi_y = \psi_T - \psi_A - \psi_{yy} \quad . \tag{34}$$

Substituting this relation for ψ_y and solving Eq. (33b) for ψ_{yy} yields

$$\psi_{yy} = \frac{5(\psi_T + \psi_B - 2\psi_A)}{(\varepsilon_y + 10)} \quad . \tag{35}$$

Substituting this expression for ψ_{yy} into Eq. (34) for ψ_y,

$$\psi_y = \frac{5(\psi_T - \psi_B) + \varepsilon_y(\psi_T - \psi_A)}{(\varepsilon_y + 10)} \quad . \tag{36}$$

Notice that for ε large, this is the same as the LD relation in Eq. (27b) for ψ_y. Since the flux on the edge of the node is linear, Eq. (27a) still applies. Substituting from Eq. (36) into Eq. (28), the quadratic-discontinuous "augmented-weighted-diamond" form is obtained, which is identical to that of the LD scheme, Eq. (30). The only difference is that the f_y are now defined as

$$f_y = \frac{(10 + \varepsilon_y) \cdot \varepsilon_y \cdot (1 + \varepsilon_x)}{(5 + \varepsilon_y)\varepsilon_y(1 + \varepsilon_x) + 3\varepsilon_x(10 + \varepsilon_y)} \quad . \tag{37}$$

A similar expression can be obtained for the x coordinate carrying out similar operations on the ψ_x equation, Eq. (7). These expressions along with the balance equation for ψ_A constitute the equations of the quadratic-discontinues QD scheme.

In this section, the "augmented-weighted-diamond" form of the LD and QD schemes has been derived simply by using the balance equations, and the polynomial expansions associated with each scheme. In general, it is expected that the positivity should be in the order DD, LD, and QD, from most positive to least positive. This is based on the positivity of the Pade' approximation used in each scheme.

VI. DISCUSSION AND RESULTS

The results of an analysis of a two-dimensional, well-logging problem investigated in Refs. 9 and 13 are shown in Figs. 1 and 2. The LL solution, which is the most accurate solution at every node refinement, is shown in both figures. The data for both figures is shown in Table 1. The absorption rate plotted is that determined in the detector of a well-logging tool. The minimum value of the mean-free path in this problem is 0.67 cm. A node size of 8 cm is then roughly 12 mean-free paths. In Fig. 1, it should not be surprising, then, that the DD solution is so ill behaved for this node size. There are so many negative flux fixups that the result is almost meaningless. At a node size of 2 cm or 3 mean-free paths, both the LL and LN solutions are well within one percent of the reference extrapolated value for detector absorption rate. Clearly, both LL and LN solutions are far more accurate than the DD solutions for reasonably sized nodes.

The LD and QD results are plotted along with the LL results in Fig. 2. Surprisingly, the LD results are slightly more accurate than the QD results for all but the smallest node size. This inaccuracy in the QD results is probably caused by the neglect of the cross term in the quadratic expansion Eq. (32). If the cross term had been retained, the system of equations for ψ_A, ψ_T, and ψ_R would have been fully coupled with all of the unknowns appearing in each of the three equations. In this case, the expression for f_y would have been extremely complicated. Neither of the discontinuous schemes is as accurate as the two nodal schemes. The advantage of the discontinuous schemes is that they can be applied to geometries other than x-y rectangular geometry where it is difficult, if not impossible, to use the nodal transport method.

In Ref. 12, it was found that in one-dimensional problems with a linear source representation, the analytic characteristic method yielded accuracies of $O(\Delta x^4)$, while the linear-discontinuous method gave $O(\Delta x^3)$. This result was the motivation for examining the QD scheme described in this paper. Since the quadratic-discontinuous scheme generates the more accurate Pade' (2,3) approximation to the exponent, it was hoped that a two-dimensional scheme would be obtained which was equivalent in accuracy to the LL nodal scheme. In future work, the full quadratic expansion will be examined.

In the present coding, the weights α in Eqs. (18a,b) and f_y in Eqs. 31 and 37 were recomputed for each phase-space point in the inner-most loop. If these weights are precomputed and stored, then each of these schemes will execute at approximately the same speed. Recall that the linear methods must compute additional moments. The storage required for one energy group is the size of the coarse mesh times the number of discrete directions in a quadrant (two dimensions).

REFERENCES

1. W. F. Walters and R. D. O'Dell, "Nodal Methods for Discrete-Ordinates Transport Problems in (x,y) Geometry," Proc. Amer. Nucl. Soc. Top. Meeting on Advances in Mathematical Methods for the Solution of Engineering Problems, Munich, FRG, 27-29 April 1981, Vol. I, pp. 115-129.

2. W. F. Walters, "Recent Developments in Nodal and Characteristic Methods in Transport Theory," Trans. Am. Nucl. Soc. 43, 611 (November 1982).

3. W. F. Walters and R. D. O'Dell, "A Comparison of Linear Nodal, Linear Discontinuous, and Diamond Schemes for Solving the Transport Equation in (x,y) Geometry," Trans. Am. Nucl. Soc. 39, 465 (November 1981).

4. B. G. Carlson and K. D. Lathrop, "Transport Theory: The Method of Discrete Ordinates," Computing Methods in Reactor Physics, p. 165, H. Greenspan, C. N. Kelber, and D. Okrent, Eds., Gordon and Breach, Science Publishers Ltd., New York (1968).

5. W. H. Reed, T. R. Hill, F. W. Brinkley, and K. D. Lathrop, "TRIPLET: A Two-Dimensional, Multigroup, Triangular Mesh, Planar Geometry, Explicit Transport Code," LA-5428-MS, Los Alamos National Laboratory (1973).

6. M. Mordant, "Some Efficient Lagrangian Mesh Finite Elements Encoded in ZEPHYR for Two-Dimensional Transport Calculations," Annals of Nuclear Energy, Vol. 8, 657-675 (1981).

7. M. Mordant, "Résolution de l'équation du transport en géométrie quelconque à deux dimensions par des méthodes d'éléments finis sur l'espace des phases," Thesis (Docteur D'Etat), Paris Orsay (1985).

8. M. Courtot, "Study of Some Numerical Schemes for Solving the Three Dimensional Transport Equation," Advances in Mathematical Methods for the Solution of Nuclear Engineering Problems, Munich, FRG, 27-29 April 1981, Vol. 1, pp. 115-129.

9. W. F. Walters, "Augmented Weighted Diamond Form of the Linear Nodal Scheme for Cartesian Coordinate Systems, Proceedings of the International Meeting on Advances in Nuclear Engineering Computational Methods, Knoxville, TN, April 9-11, Vol. II, pp. 452-460. (Also to be published with additional results in Nucl. Sci. Eng.)

10. A. Badruzzaman, "An Efficient Algorithm for Nodal-Transport Solutions in Multidimensional Geometry," Nucl. Sci. Eng. 64, 281, (1985).

11. R. D. Lawrence, "Progress in Nodal Methods for the Solution of the Neutron Diffusion and Transport Equations," to be published in Progress in Nuclear Energy.

12. E. W. Larsen and P. Nelson, "Finite-Difference Approximations and Superconvergence for Discrete-Ordinate Equations in Slab Geometry," SIAM J. Numer. Anal. 19, No. 2, p. 334, April 1982.

13. J. J. Ullo, J. J. Dorning, H. L. Dodds, and R. E. Pevey, "A Comparison of Nodal Transport Methods Based on Exponential and Polynomial Expansions," Trans. Am. Nucl. Soc. 43, 367 (November 1982).

TABLE 1

Absorption Rate in Detector

Method	Absorption Rate n/sec $\times 10^5$				
	LN	DD	DD	LD	QD
Node Size (cm.)					
8.0	9.8605	10.475	14.987	11.772	12.112
4.0	9.7785	9.89515	8.4679	10.116	10.246
2.0	9.6874	9.7009	9.3142	9.7468	9.7537
1.0	9.6429	9.6440	9.5413	9.6579	9.6519
.50			9.6087		
.25			9.6257		

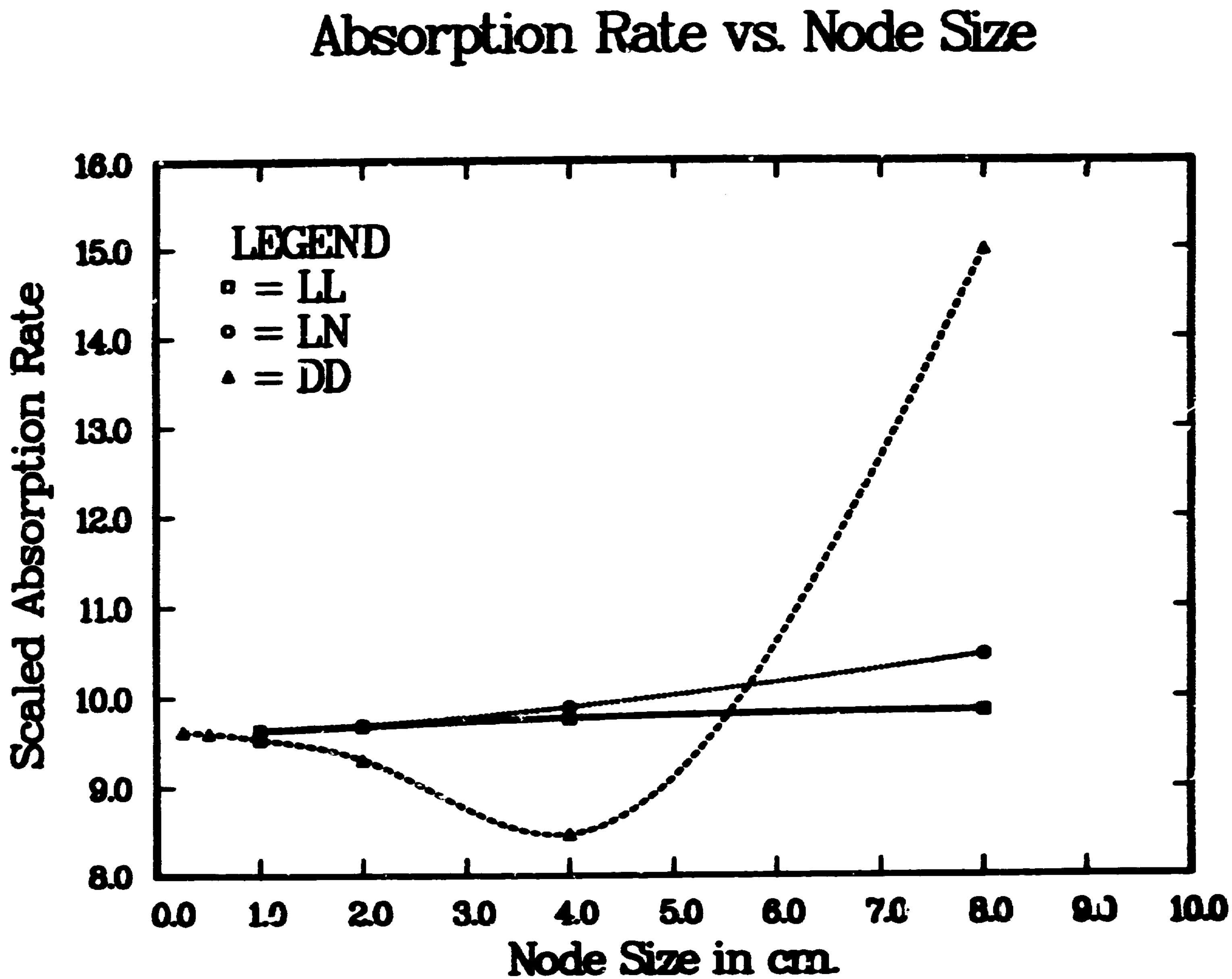
Absorption Rate vs. Node Size
LEGEND
□ = LL
○ = LN
▲ = DD
Scaled Absorption Rate
16.0
15.0
14.0
13.0
12.0
11.0
10.0
9.0
8.0
0.0
1.0
2.0
3.0
4.0
5.0
6.0
7.0
8.0
9.0
10.0
Node Size in cm.

Figure 1

Absorption Rate vs. Node Size

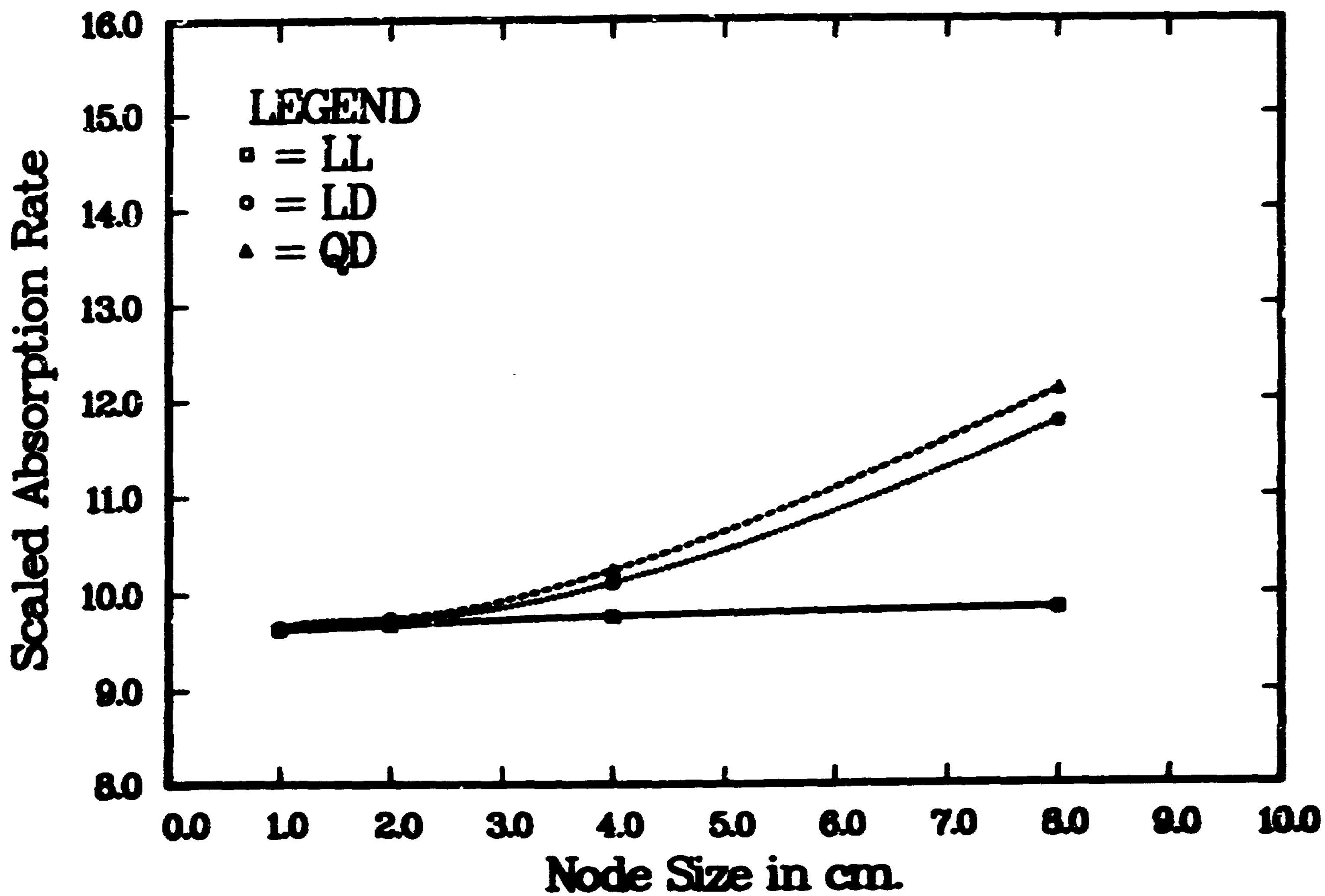

Figure 2